

Memory effects in a sequence of measurements of non-commuting observables

Sophia M. Walls and Ian J. Ford

*Department of Physics and Astronomy, University College London,
Gower Street, London, WC1E 6BT, United Kingdom*

We use continuous, stochastic quantum trajectories within a framework of quantum state diffusion (QSD) to describe alternating measurements of two non-commuting observables. Projective measurement of an observable completely destroys memory of the outcome of a previous measurement of the conjugate observable. In contrast, measurement under QSD is not projective and it is possible to vary the rate at which information about previous measurement outcomes is lost by changing the strength of measurement. We apply our methods to a spin 1/2 system and a spin 1 system undergoing alternating measurements of the S_z and S_x spin observables. Performing strong S_z measurements and weak S_x measurements on the spin 1 system, we demonstrate return to the same eigenstate of S_z to a degree beyond that expected from projective measurements and the Born rule. Such a memory effect appears to be greater for return to the ± 1 eigenstates than the 0 eigenstate. Furthermore, the spin 1 system follows a measurement cascade process where an initial superposition of the three eigenstates of the observable evolves into a superposition of just two, before finally collapsing into a single eigenstate, giving rise to a distinctive pattern of evolution of the spin components.

I. INTRODUCTION

Non-commuting or conjugate observables are considered to be a hallmark of quantum mechanics. Measurement of one is conventionally taken to erase any information about its conjugate partner [1, 2]. Figure 1 demonstrates how a σ_z measurement outcome at Stern-Gerlach device 1 (STG1) acting on a beam of spin 1/2 particles is ‘forgotten’ because of the measurement of non-commuting observable σ_x at STG2. The system is measured at STG1 to be in the +1 eigenstate of σ_z yet the second σ_z measurement at STG3 has an equal likelihood of ± 1 outcomes. Naturally this is reflected in the mathematics by the fact that the $|+\rangle_x$ and $|-\rangle_x$ spin 1/2 eigenstates can be written as an equal amplitude superposition of $|+\rangle_z$ and $|-\rangle_z$ eigenstates: $|+\rangle_x = \frac{1}{\sqrt{2}}(|+\rangle_z + |-\rangle_z)$, where the suffixes indicate the measured observable.

Whilst conventional quantum mechanics focuses on projective, instantaneous measurements, and average outcomes which mask what happens during single mea-

surements, more generalised descriptions of measurement exist as well as a wider scope of measurement types [2]. Weak measurements are a frequently cited example [3–10]. Whilst projective measurements extract maximum information about a system, weak measurements extract partial information, causing less disturbance to the system itself. The system collapses over a finite time frame or may not completely collapse at an eigenstate at all.

Weak measurements relax many quantum foundational principles related to conjugate variables. For example Calderón-Losada *et al* were able to assign simultaneously measured values of two non-commuting observables to particles in an EPR (Einstein-Podolsky-Rosen) experiment using weak measurements [11]. Rozema *et al* demonstrated a violation of Heisenberg’s uncertainty principle using weak measurement [4]. Similarly, weak measurements have been used to establish ‘weak value’ correlators across measurement outcomes or to demonstrate violations of the Leggett-Garg or Bell inequalities [12–21]. Non-commuting observables have also been studied in the context of testing quantumness, quantum randomness using the Kochen-Specker theorem and the relation between the EPR settings and Heisenberg’s uncertainty principle [22–27]. Hossenfelder *et al* proposed a scheme where a sequence of measurements of non-commuting observables might be used to examine correlations in measurement outcomes of the same observable at different times [28].

In this paper we study the destruction of prior information in a sequence of alternating measurements of non-commuting observables. We consider how such information loss may be reduced if weak measurements are used instead of strong, projective ones.

In order to investigate such a scenario, a framework where measurement occurs over a finite amount of time is required, one where single evolution pathways for a system may be tracked [29–31]. Many techniques exist for generating quantum trajectories, such as the Feynman-

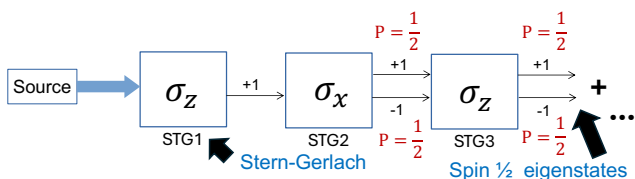


Figure 1. A demonstration of memory erasure in a sequence of projective measurements of non-commuting observables σ_z and σ_x . Stern-Gerlach devices 1 (STG1) and 3 (STG3) conduct σ_z measurements whilst STG2 performs a σ_x measurement. The system is measured to be in the +1 state at STG1 but in a second σ_z measurement at STG3 the system has equal probability of being in the +1 or -1 state. The cause of this ‘forgetting’ is the projective σ_x measurement at STG2.

Vernon path integral formalism, hierarchical equations of motion, and various unravellings of the Lindblad master equation [32–40]. The Liouville-von Neumann equation is a further example, though it does not preserve positivity and thus the trajectories generated cannot be considered as physically realistic [33–36, 41, 42].

In this work we generate stochastic, continuous and diffusive quantum trajectories using quantum state diffusion (QSD) [43]. Quantum state diffusion is a framework which describes measurement as a continuous and gradual process. Similarly to Gisin and Percival, we interpret measurement in this framework to be a consequence of a system-environment interaction, where we consider the environment to act as a (classical) measurement apparatus [43, 44]. This is to be contrasted with Gambetta, Wiseman and Jacobs who consider the system’s state to be conditioned on the measured state of the environment which then contains information about the state of the system [32, 40, 45, 46].

The interaction with the environment drives the system towards an eigenstate of the observable in a continuous and diffusive manner, such that the completion of measurement takes a finite amount of time [47, 48]. System evolution is described by a stochastic differential equation (SDE) that includes noise terms representing its interactions with the environment and hence the effect of measurement. In the absence of interactions with the environment, evolution is described by the (deterministic) von Neumann equation. The SDE generates single stochastic trajectories and the average over all trajectories generated by the environmental noise yields the Lindblad master equation [48]. Many different unravellings of the Lindblad master equation exist, corresponding to different measurement schemes such as direct photon detection, heterodyne or homodyne measurements and more recently, the jump-time unravelling. QSD is an example of a continuous unravelling of the Lindblad master equation.

The possibility of simultaneous measurement of conjugate variables through weak measurement has proved to have a useful application in direct measurement of the elements of a density matrix of a quantum system and quantum state tomography [6, 49–53], as well as quantum error correction and quantum cybersecurity [54–57] which rely on simultaneous or alternating measurements of non-commuting observables. Quantum cybersecurity algorithms and cryptography which rely on the principle that measurements of conjugate observables destroy information about one another, could be left vulnerable to attack by the possibility of incomplete measurement [4, 10, 14, 15, 27, 51, 58–64].

We employ stochastic quantum trajectories to investigate memory effects in a series of alternate measurements of two non-commuting observables. We perform strong measurements of the first observable and weak measurements of the second. Incomplete collapse of the system to an eigenstate of the second observable could preserve information about the first observable. For example, in

Fig. 1, if the measurement at STG2 were weak, the system might return more often than expected at STG3 to the same eigenstate of σ_z it was in at STG1. Memory effects in incomplete measurements have been studied before using quantum trajectories in relation to the partial quantum Zeno effect, for example [65, 66], and there have been investigations of the reversal of quantum measurements whereby the system returns to a previous state after a partial collapse [31, 67–69]. Such memory effects can be observed only when studying single system evolution pathways as opposed to average system behaviour, and with continuous and gradual wavefunction collapse instead of instantaneous and discontinuous evolution.

We study two separate systems: a spin 1/2 system and a spin 1 system, both undergoing alternating measurements of spin component S_z and S_x observables. We consider cases of equal measurement strength of both observables, and more particularly a situation involving strong S_z measurements and a varying strength of S_x measurement. We explore system return to the same eigenstate of S_z , given a particular strength of measurement of S_x , and the pattern of system exploration of its parameter space.

The plan for the paper is as follows: section II outlines the QSD framework and general SDE used to generate quantum trajectories; section III introduces the SDEs specific to the spin 1/2 system and the spin 1 system as well as describing the protocol for generating sequential measurements of non-commuting observables; and finally sections IV and V present our results and conclusions.

II. QUANTUM STATE DIFFUSION AND STOCHASTIC LINDBLAD EQUATIONS

Measurement in QSD arises from an interaction between an open quantum system and a classical environment, the effect of which is to evolve the system continuously and stochastically towards one of the eigenstates of the measured observable. Our interpretation is that the uncertain initial state of the environment, together with complex interaction dynamics, is responsible for the stochastic evolution of the system state, rather like the stochastic evolution of an open classical system. In such circumstances the open quantum system state can be modelled using a randomly evolving (reduced) density operator, or matrix, ρ . We describe the mean (Markovian) evolution of ρ in a time increment dt using a superoperator $\hat{S}[\rho]$ defined in terms of Kraus operators M_j [2, 70]:

$$\begin{aligned} \hat{S}[\rho(t)] &= \sum_j M_j(dt)\rho(t)M_j^\dagger(dt) \\ &= \sum_j p_j \frac{M_j(dt)\rho(t)M_j^\dagger(dt)}{\text{Tr}(M_j(dt)\rho(t)M_j^\dagger(dt))}, \end{aligned} \quad (1)$$

where we have written $p_j = \text{Tr}(M_j \rho M_j^\dagger)$. Such an evolution is positive and trace-preserving when the Kraus operators satisfy the completeness condition $\sum_j M_j^\dagger M_j = \mathbb{I}$. The evolution is Markovian since the future state of the system depends only on its current state $\rho(t)$.

Equation (1) can be interpreted as an average over transitions of the current state of the system $\rho(t)$ to one of several possible states $M_j \rho(t) M_j^\dagger / \text{Tr}(M_j \rho(t) M_j^\dagger)$ in the time interval dt , each taking place with probability $p_j = \text{Tr}(M_j \rho(t) M_j^\dagger)$ [47]. To generate diffusive, continuous trajectories we employ Kraus operators that differ incrementally from (proportionality to) the identity:

$$M_j \equiv M_{k\pm} = \frac{1}{\sqrt{2}}(\mathbb{I} + A_{k\pm}), \quad (2)$$

where

$$A_{k\pm} = -iH_s dt - \frac{1}{2}L_k^\dagger L_k dt \pm L_k \sqrt{dt}. \quad (3)$$

The index k specifies Lindblad channels, each of which is associated with two Kraus operators labelled by \pm [46, 47, 71–73]. The system Hamiltonian is denoted by H_s and the Lindblad operators by L_k .

In QSD we consider an ensemble of states that the system could adopt, with the average density matrix over the ensemble then denoted as $\bar{\rho}(t)$. A single member of the ensemble evolves in a timestep according to the action of a single Kraus operator M_j , representing the transition

$$\rho(t + dt) = \rho(t) + d\rho = \frac{M_j \rho(t) M_j^\dagger}{\text{Tr}(M_j \rho(t) M_j^\dagger)}, \quad (4)$$

and a sequence of transitions then yields a stochastic trajectory. Note that such a map with a Kraus operator of the form given in Eqs. (2) and (3) has been demonstrated to preserve positivity [47]. The average evolution over all possible system transitions may then be shown to satisfy the Lindblad master equation [71]

$$d\bar{\rho} = -i[H_s, \bar{\rho}]dt + \sum_k \left(L_k \bar{\rho} L_k^\dagger - \frac{1}{2} \{L_k^\dagger L_k, \bar{\rho}\} \right) dt, \quad (5)$$

while a single trajectory is a solution to the following SDE for quantum state diffusion:

$$d\rho = -i[H_s, \rho]dt + \sum_k \left((L_k \rho L_k^\dagger - \frac{1}{2} \{L_k^\dagger L_k, \rho\}) dt + (\rho L_k^\dagger + L_k \rho - \text{Tr}[\rho(L_k + L_k^\dagger)]\rho) dW_k \right). \quad (6)$$

The evolution of ρ is thus an Itô process with Wiener increments dW_k , one for each Lindblad operator or channel k [43, 48], and arising from system-environment interactions.

It is well known that the quantum operation in Eq. (1) is invariant under a unitary transformation of the Kraus operators: $M_j \rightarrow M'_j = \sum_m U_{jm} M_m$. Thus the Kraus operator representation in Eqs. (2) and (3) would not appear to be unique. For example, the same Lindblad equation for the evolution of the mean density matrix $\bar{\rho}(t)$ would emerge for Kraus operator pairs: $M'_{k\pm} = \frac{1}{\sqrt{2}}(M_{k+} \pm M_{k-})$ or more explicitly $M'_{k+} = \mathbb{I} - iH_s dt - \frac{1}{2}L_k^\dagger L_k dt$ and $M'_{k-} = L_k \sqrt{dt}$.

However, what is unique about the choice of $M_{k\pm}$ is that they generate continuous trajectories: they both are proportional to the identity when $dt \rightarrow 0$, while M'_{k-} , in contrast, generates jumps. Since we take the view that individual trajectories of the density matrix must be continuous, arising from a stochastic Lindblad equation that is diffusive, unitary freedom in the choice of Kraus operators is not available here.

III. SYSTEM SPECIFICATION AND DYNAMICS

For simplicity we consider a system with $H_s = 0$ and two Lindblad operators $L_z = aS_z$ and $L_x = bS_x$ where the S_i are spin component operators and $a(t)$ and $b(t)$ are scalar, time-dependent coefficients representing system-environment couplings. Each interaction is associated with Wiener increments dW_z and dW_x , respectively, in the dynamics. When inserted into Eq. (6), we obtain the following SDE [73]

$$d\rho = a^2 \left(S_z \rho S_z - \frac{1}{2} \rho S_z^2 - \frac{1}{2} S_z^2 \rho \right) dt + b^2 \left(S_x \rho S_x - \frac{1}{2} \rho S_x^2 - \frac{1}{2} S_x^2 \rho \right) dt + a (\rho S_z + S_z \rho - 2\langle S_z \rangle \rho) dW_z + b (\rho S_x + S_x \rho - 2\langle S_x \rangle \rho) dW_x, \quad (7)$$

where $\langle S_i \rangle = \text{Tr}(\rho S_i)$. Note that we do not consider $\langle S_i \rangle$ to be an ‘expectation value’ in the conventional sense: namely as a statistical property of the dynamics. Rather we regard it as a stochastically evolving physical attribute of the quantum state of the system [47].

In order to generate a sequence of alternating measurements of the non-commuting observables S_z and S_x we take the system-environment couplings $a(t)$ and $b(t)$ to be time-varying box functions subject to $a(t) \neq 0, b(t) = 0$ and vice-versa (see Figure 2). The period of the box function T in conjunction with a_{max} (the maximum value of $a(t)$) defines the S_z measurement strength M_z , whilst b_{max} (the maximum value of $b(t)$) defines the S_x measurement strength M_x :

$$M_z = a_{max}^2 \frac{T}{2}, \quad M_x = b_{max}^2 \frac{T}{2}. \quad (8)$$

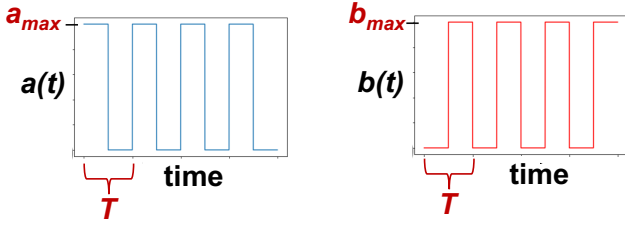


Figure 2. System-environment couplings $a(t)$ and $b(t)$ for the observables S_z and S_x , respectively. In order to produce alternating measurements of the non-commuting observables, they are modelled as box functions such that when $a(t) = 1$, $b(t) = 0$ and vice-versa. The measurement strengths are defined by the maximum values of $a(t)$ and $b(t)$ (a_{max} and b_{max}) and the period of the box function T , as given in Eq. (8).

The period of measurement of one of the observables is half of the box function period.

A. Spin 1/2 system

The density matrix of a spin 1/2 system can be written $\rho = \frac{1}{2}(\mathbb{I} + \mathbf{r} \cdot \boldsymbol{\sigma})$ where $\mathbf{r} = (r_x, r_y, r_z)$ is the coherence vector $\mathbf{r} = Tr(\rho\boldsymbol{\sigma})$ and $\boldsymbol{\sigma} = (\sigma_x, \sigma_y, \sigma_z)$ is a vector of Pauli matrices. Using $d\mathbf{r} = Tr(d\rho\boldsymbol{\sigma})$, and Eq. (7), we can derive SDEs for the coherence vector components. We choose $r_y = 0$, $dr_y = 0$ for simplicity and obtain the following SDEs, using $S_z = \frac{1}{2}\sigma_z$ and $S_x = \frac{1}{2}\sigma_x$ in Eq. (7) [53]:

$$\begin{aligned} dr_z &= 2a(1 - r_z^2) dW_z - 2b^2 r_z dt - 2br_z r_x dW_x, \\ dr_x &= 2b(1 - r_x^2) dW_x - 2a^2 r_x dt - 2ar_x r_z dW_z. \end{aligned} \quad (9)$$

Stochastic trajectories in terms of the coherence vector components (r_x, r_z) are then generated using these SDEs. Note that r_x, r_z define the density matrix at each point in time since $r_y = 0$.

B. Spin 1 system

The generalised Bloch sphere formalism is used to represent the density matrix of a spin 1 system. This permits any 3×3 density matrix to be written in terms of the Gell-Mann matrices λ_i through

$$\rho = \frac{1}{3}(\mathbb{I} + \sqrt{3}\mathbf{R} \cdot \boldsymbol{\lambda}), \quad (10)$$

where $\mathbf{R} = (s, m, u, v, k, x, y, z)$ is an eight dimensional coherence (or Bloch) vector and the Gell-Mann matrices form the elements of the vector $\boldsymbol{\lambda} = (\lambda_1, \lambda_2, \lambda_3, \lambda_4, \lambda_5, \lambda_6, \lambda_7, \lambda_8)$ (see Appendix A for details). SDEs for the evolution of the coherence vector

components can then be constructed and are given in Appendix A.

The S_x and S_z operators for a spin 1 system each have three eigenstates: $| -1 \rangle_x, |0 \rangle_x, |1 \rangle_x$ and $| -1 \rangle_z, |0 \rangle_z, |1 \rangle_z$, respectively. The spin components $\langle S_x \rangle$, $\langle S_y \rangle$ and $\langle S_z \rangle$ can be written:

$$\begin{aligned} \langle S_x \rangle &= \sqrt{\frac{2}{3}}(x + s) \\ \langle S_y \rangle &= \sqrt{\frac{2}{3}}(m + y) \\ \langle S_z \rangle &= \frac{u}{\sqrt{3}} + z. \end{aligned} \quad (11)$$

We take the initial state of the system to be an equal mixture of the three eigenstates of S_z : $|\rho_{start}\rangle = \frac{1}{3}(|1\rangle_z \langle 1|_z + |0\rangle_z \langle 0|_z + | -1\rangle_z \langle -1|_z)$. As a result, $\langle S_y \rangle$ remains zero throughout, as well as the variables k, m and y , leaving five variables as active participants in the dynamics. Stochastic quantum trajectories are then generated using the SDEs for these variables. Rather than imagining their evolution in the five dimensional space of (s, u, v, x, z) , we project them into the $(\langle S_x \rangle, \langle S_z \rangle)$ space which offers a more insightful understanding of the dynamics. Note that the eigenstates $|0\rangle_x$ and $|0\rangle_z$ both lie at $\langle S_x \rangle = 0, \langle S_z \rangle = 0$, but are orthogonal. Indeed $\langle S_x \rangle = 0, \langle S_z \rangle = 0$ can describe many different states, including the initial state of the system.

IV. DWELL TIMES AND CUMULATIVE PROBABILITY DENSITIES

We wish to understand how alternating measurements of conjugate observables destroy information about one another. As illustrated in Figure 1, conventional projective measurement at STG2 implies that the information gathered at STG1 is ‘forgotten’ such that measurement of the same observable at STG3 yields an uncorrelated outcome. Weak measurements might not cause the system to collapse completely to an eigenstate of S_x since information about the system is being extracted at a slower rate. As a result, subsequent S_z measurement might be biased towards a return to its previous state.

From the quantum trajectories, we produce a time series of measurement outcomes of S_z . The time parameter is defined by the count of S_z measurements that have taken place in the sequence of alternating measurements of S_x and S_z . For each of the eigenstates of S_z , we can calculate the number of consecutive returns to the same eigenstate and we shall refer to this as the *dwell time*. We calculate how long the system *dwells* at a particular eigenstate in spite of attempts to measure a conjugate observable. Figure 3 illustrates an example: at STG7 the system is found to take the -1 eigenstate, and therefore the dwell time in the $+1$ eigenstate since its initiation at STG1, is 3. We investigate this with a high strength of measurement of S_z while varying the strength of the S_x measurements.

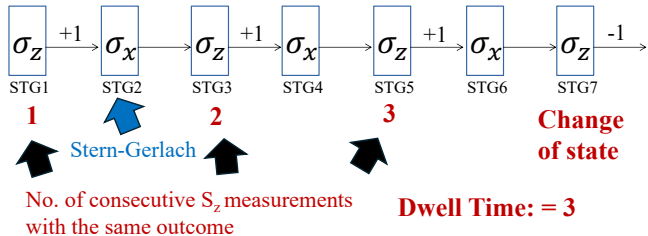


Figure 3. Investigating the number of repeated S_z measurement outcomes before a spin 1/2 system is able to adopt a different S_z eigenstate.

We perform dwell time calculations using strong S_z measurements and a range of strengths of S_x measurements. In this situation, there is ample time for the system to approach very close to an eigenstate of S_z for every measurement, therefore the *dwell time* does not depend on a precise definition of eigenstate adoption. The dwell time is expected to depend on the strength of measurement of S_x .

We also use trajectories to generate cumulative probability densities in the $(\langle S_x \rangle, \langle S_z \rangle)$ plane to illustrate the behaviour of the system. We do this for equal strength of measurement of the two observables.

A. Spin 1/2 system

Numerical trajectories of r_x and r_z were generated for the spin 1/2 system undergoing sequential, alternating measurements of σ_x and σ_z . We begin with a case where the measurement strengths of σ_x and σ_z are equal. An example trajectory is shown in Figure 4. The system begins at the centre of the circle in the totally mixed state. An initial σ_z measurement is performed with equal probability of arriving at either $r_z = 1$ or $r_z = -1$. As σ_x and σ_z measurements are performed, the system purifies and evolves towards the circumference of the circle, where it remains. The σ_x eigenstates lie at the equator, equidistant from the σ_z eigenstates at the poles. Starting from one of the σ_x eigenstates there is an equal chance for the system to travel towards either of the σ_z eigenstates during an σ_z measurement (and vice-versa).

When the measurement strength is weak, the measurement process may be incomplete: the system may not arrive at the eigenstate of the observable that is being measured. Figures 5a and b illustrate a σ_z measurement of the system, between times 18 and 19, that causes the system to evolve towards the $r_z = +1$ eigenstate while r_x tends towards zero. A σ_x measurement is then performed between times 19 and 20, leading the system away from $r_x = 0$, but it does not unequivocally arrive at an eigenstate of σ_x . Within the time interval 20-21, a second σ_z measurement is performed and the system moves back to the $r_z = +1$ eigenstate it adopted when the first σ_z measurement was conducted during the time interval

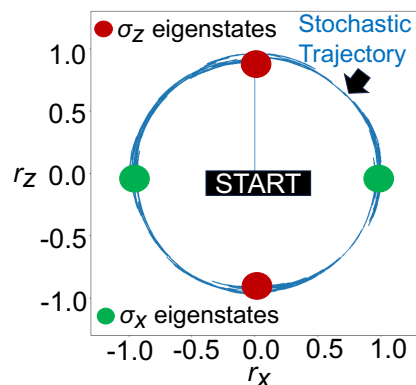


Figure 4. An example stochastic trajectory (in blue) of the coherence vector components (r_x, r_z) for the spin 1/2 system, starting in the mixed state at the centre of the Bloch sphere. When a measurement is performed, the system is purified and travels towards the circumference, where it remains.

18-19. A σ_x measurement is made once again between times 21 and 22, causing the system to travel towards a σ_x eigenstate but again it is not successful in reaching it. As a result, when a third σ_z measurement is performed in interval 22-23, the system again returns to the same eigenstate as in the previous two measurements of σ_z . Since the σ_x measurements fail to take the system to a σ_x eigenstate, the system is allowed to return to the same eigenstate of σ_z multiple times.

This can also be understood using Figure 4. Let us take the system to be in the vicinity of the north pole after a σ_z measurement. A subsequent σ_x measurement might not bring the system to an eigenstate in the time available, so that the system remains in the top half of the circle. This means that when a second σ_z measurement is conducted, the system is more likely to return to the $r_z = +1$ eigenstate than the $r_z = -1$ eigenstate, since it is closer. This is how memory might emerge.

Cumulative probability densities over the (r_x, r_z) plane are illustrated in Figure 6 for $M_x = M_z$. As the measurement strengths are increased, the system spends more time in the vicinity of the eigenstates of σ_z and σ_x and the time spent in each of their respective eigenstates is equal (Figures 6 a and b). As the measurement strengths are reduced, the system explores the circumference of the circle more uniformly (Figure 6 d) or shows a bias towards certain eigenstates of the observables than others. For example, Figure 6c shows a tendency to spend more time at the $r_x = +1$ eigenstate of σ_x and the $r_z = -1$ eigenstate of σ_z .

The stabilisation of the system at a particular eigenstate of σ_z , illustrated in Figure 5, is now investigated

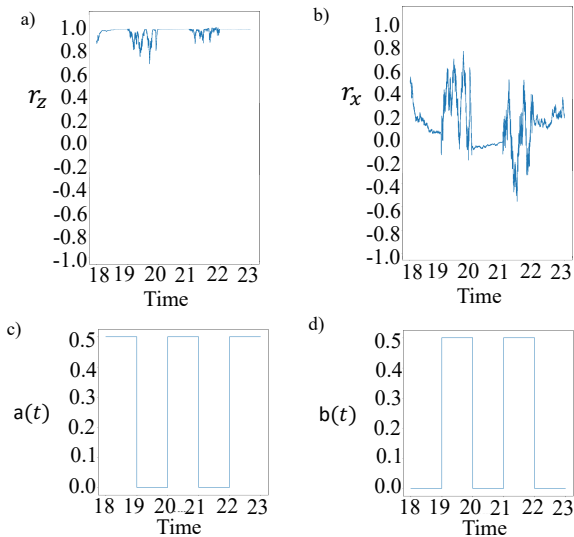


Figure 5. a) and b) An example trajectory illustrating how the coherence vector components r_z and r_x vary with time. c) evolution of the coupling $a(t)$ and d) the coupling $b(t)$. Measurement strengths: $M_x = M_z = \frac{1}{4}$ and time-step 0.0001 were used. A measurement of σ_z starts at times 18, 20 and 22, whilst a measurement of σ_x starts at 19, 21 and 23.

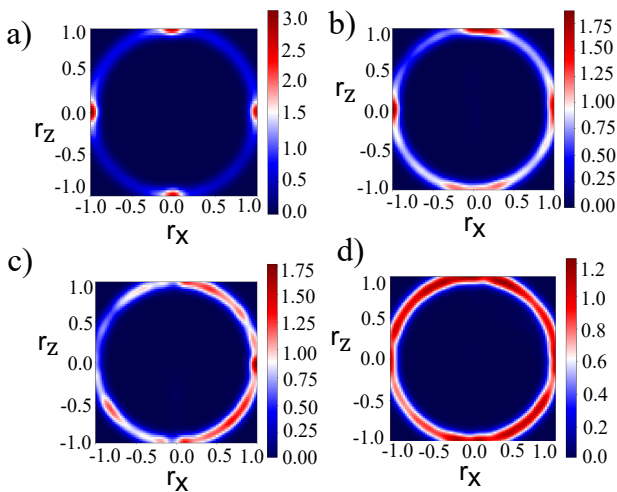


Figure 6. Color. Cumulative probability densities in the (r_x, r_z) phase space, arising from continuous stochastic trajectories for the spin 1/2 system under sequential measurement. Measurement strengths $M_x = M_z$ are as follows: a) 1, b) 0.5, c) 0.25, d) 0.1875. Duration 200, time-step 0.0001.

by employing strong σ_z measurements and weak σ_x measurements in the sequence of alternating measurements. We calculate the mean dwell time: the average number of times that the system is able to return to the same eigenstate of σ_z . Figure 7 illustrates the mean dwell time for the spin 1/2 system for both eigenstates of σ_z , and for varying σ_x measurement strength.

From Figure 7 it can be seen that the mean dwell time

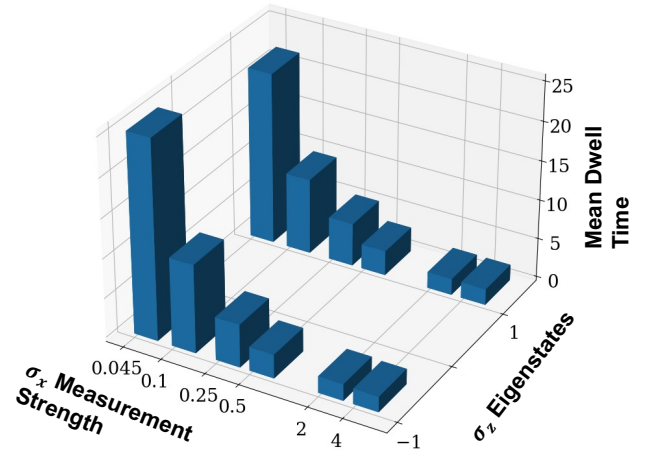


Figure 7. The mean dwell time for the spin 1/2 system for the two eigenstates of σ_z and for a range of σ_x measurement strengths. The dwell time is the number of consecutive σ_z measurements for which the system is able to return to the same eigenstate. 5000 σ_z measurements were used to calculate the mean. The σ_z measurement strength was 32.

for both eigenstates increases as the σ_x measurement strength is decreased whilst keeping the σ_z measurement strength high, indicating that the system is more biased towards return to the same eigenstate of σ_z for longer measurement sequences. The dwell time is roughly equal for both eigenstates for all σ_x measurement strengths.

B. Spin 1 system

Numerical trajectories for the parameters of the spin 1 density matrix were used to compute trajectories for the spin components $(\langle S_x \rangle, \langle S_z \rangle)$. Figure 8 depicts an example trajectory with the S_x eigenstates illustrated in pink: the $|\pm 1\rangle_x$ eigenstates at the equator and the $|0\rangle_x$ eigenstate at the centre. The S_z eigenstates are shown in green: the $|\pm 1\rangle_z$ eigenstates at the poles and the $|0\rangle_z$ eigenstate also at the centre, noting that it is orthogonal to $|0\rangle_x$.

The system is initiated at the centre of the circle, in the mixed state $\rho_{\text{start}} = \frac{1}{3}(|1\rangle_z\langle 1|_z + |0\rangle_z\langle 0|_z + |-1\rangle_z\langle -1|_z)$ such that there is an equal probability of reaching any of the S_z eigenstates following an S_z measurement. The trajectory shows an intriguing avoidance of certain regions, giving rise to a petal-like pattern of exploration. We find that the pattern is influenced by combinations of two of the three eigenstates of S_x and of S_z . For example, in Figure 9a a superposition of the $|+1\rangle_z$ and $|0\rangle_z$ eigenstates is represented by the red ellipse in the upper section and a superposition of the $|-1\rangle_z$ and $|0\rangle_z$ eigenstates by the red ellipse in the lower section. The horizontal straight line in Figure 9b illustrates a super-

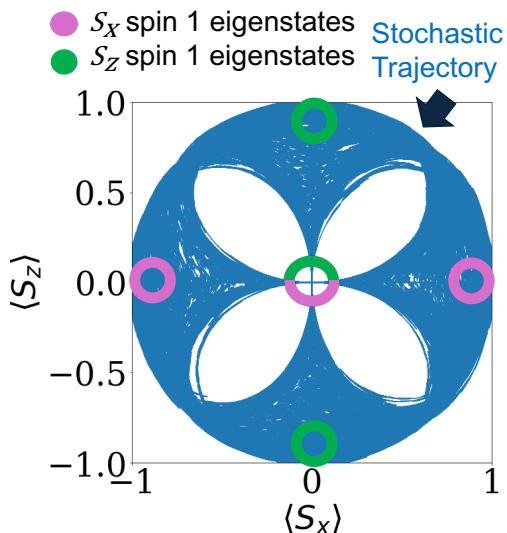


Figure 8. An example trajectory of the spin 1 system, starting in the mixed state $\rho_{\text{start}} = \frac{1}{3}(|1\rangle_z\langle 1|_z + |0\rangle_z\langle 0|_z + |-1\rangle_z\langle -1|_z)$ illustrated in terms of the spin components ($\langle S_x \rangle, \langle S_z \rangle$). Measurement strength: $M_x = M_z = 8$, duration 500, time-step 0.0001. The S_x eigenstates are illustrated in pink and the S_z eigenstates in green. The $|\pm 1\rangle_x$ eigenstates lie at the equator and the $|\pm 1\rangle_z$ eigenstates at the poles. The $|0\rangle_z$ and the $|0\rangle_x$ eigenstates are both at the centre but are mutually orthogonal.

position between the $|1\rangle_x$ and $|-1\rangle_x$ eigenstates and the vertical line a superposition between the $|1\rangle_z$ and $|-1\rangle_z$ eigenstates.

Similarly, in Figure 9c a superposition of the $|+1\rangle_x$ and $|0\rangle_x$ eigenstates is illustrated by the red ellipse in the right hand section and a superposition of the $|-1\rangle_x$ and $|0\rangle_x$ eigenstates by the red ellipse on the left.

The boundaries of the avoided petal-like regions correspond to combinations of the red ellipses in Figures 9a and 9c. We argue that this pattern stems from the way in which the spin 1 system collapses to an eigenstate.

To understand this, consider a situation where the system takes the $|-1\rangle_z$ eigenstate after undergoing a measurement of S_z , establishing a starting point for a subsequent measurement of S_x , an example pathway for which is depicted in Figure 10a. From the $|-1\rangle_z$ eigenstate, an S_x measurement leads to probabilities of $\frac{1}{4}$, $\frac{1}{2}$ and $\frac{1}{4}$ for collapsing to the $|1\rangle_x$, $|0\rangle_x$ and $|-1\rangle_x$ eigenstates, respectively. Figure 10b illustrates how the probabilities of collapse to the eigenstates of S_x evolve over the course of the measurement. Initially the probabilities are indeed those defined by the $|-1\rangle_z$ eigenstate expressed in the S_x basis. The system evolves in this case by first eliminating the probability of collapse to $|-1\rangle_x$, taking the system to a superposition between the $|1\rangle_x$ and $|0\rangle_x$ eigenstates alone, depicted in Figures 9c as a red ellipse on the right and in Figure 10a as a green semi-elliptical locus. The system remains in a superposition of the two eigenstates, and confined to the green locus, until collapsing to only

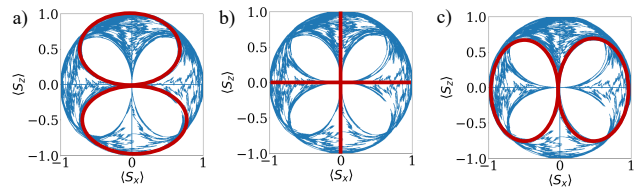


Figure 9. Color. Example trajectory of the spin 1 system in the space of spin components ($\langle S_x \rangle, \langle S_z \rangle$), with measurement strengths: $M_x = M_z = 8$, duration 80, time-step 0.0001. a) The red ellipse in the upper section is the locus of a superposition of $|+1\rangle_z$ and $|0\rangle_z$ eigenstates, and the lower red ellipse a superposition of $|-1\rangle_z$ and $|0\rangle_z$. b) The vertical red line represents superposition between $|-1\rangle_z$ and $|1\rangle_z$ eigenstates and the horizontal line a superposition between $|-1\rangle_x$ and $|1\rangle_x$. c) The red ellipse on the left is a locus of a superposition between $|-1\rangle_x$ and $|0\rangle_x$ eigenstates, and the red ellipse on the right is a superposition between $|1\rangle_x$ and $|0\rangle_x$.

one of them, which in Figure 10a happens to be the $|1\rangle_x$ eigenstate. Figure 10b reflects this final collapse by showing the probabilities of the $|1\rangle_x$ and the $|0\rangle_x$ eigenstates rising to one and falling to zero, respectively.

We could think of this as a ‘collapse cascade’: a multistep process of wavefunction collapse. The system collapses first onto a subspace spanned by two of the eigenstates of the observable, before ultimately completely collapsing at one eigenstate. The petal regions in Figure 8 are avoided because once the system has arrived at a point on one of the red ellipses depicted in Figure 9, typically coming from the region outside the petal-like regions, then a move within the petals would mean re-introducing a non-zero amplitude for the third eigenstate of the observable. This would be contrary to the nature of the measurement dynamics. Indeed, when in a two eigenstate superposition, the drift and diffusion coefficients along the direction of the eigenstate with zero amplitude are both zero. Thus eigenstates in the superposition are typically eliminated one by one.

Note that if the system had started in the $|0\rangle_z$ eigenstate, then it would already be in a superposition of just $|1\rangle_x$ and $|-1\rangle_x$ since $|0\rangle_z = -\frac{1}{\sqrt{2}}|1\rangle_x + \frac{1}{\sqrt{2}}|-1\rangle_x$. The system would then evolve along the horizontal line depicted in Figure 9b, leading towards one or other of $|\pm 1\rangle_x$. This situation therefore skips step one of the measurement collapse cascade. Entering the petal-like regions would still represent a regression in the measurement collapse process through introducing a non-zero amplitude for the $|0\rangle_x$ eigenstate, and is incompatible with the dynamics.

As with the spin 1/2 system, we can use a long trajectory to compute a cumulative probability density that characterises the evolution of the spin 1 system in the space of the spin components ($\langle S_x \rangle, \langle S_z \rangle$). Figure 11 depicts how the cumulative probability density varies with measurement strength. For measurement strengths of 8 for both observables, shown in Figure 11a, the highest probability density is found around the eigenstates of S_x

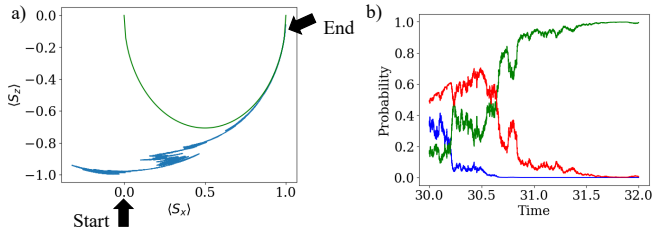


Figure 10. a) An example of a collapse cascade in the spin 1 system. The system begins at the $| - 1 \rangle_z$ eigenstate and then undergoes a S_x measurement. The green semi-elliptical locus represents a superposition between the $| 0 \rangle_x$ and $| 1 \rangle_x$ eigenstates. During the S_x measurement, the system moves first to a point on this locus, as the probability of the $| - 1 \rangle_x$ eigenstate decreases to zero. The system then remains on the green locus until collapsing at the $| 1 \rangle_x$ eigenstate. b) The evolving probabilities of the $| 1 \rangle_x$, $| 0 \rangle_x$ and $| - 1 \rangle_x$ eigenstates of S_x in green, red and blue, respectively. S_x measurement strength 2.

and S_z . In accordance with the Born rule, the probability around the centre is twice as large as around the other eigenstates, since this is the location of both the $| 0 \rangle_x$ and the $| 0 \rangle_z$ eigenstates. As the measurement strength is decreased, the probability density spreads away from the eigenstates such as in Figures 11e and f. It is notable, in particular, that the $| 0 \rangle_x$ and the $| 0 \rangle_z$ eigenstates are visited significantly less frequently than the $| \pm 1 \rangle_x$ and $| \pm 1 \rangle_z$ eigenstates when the measurement strength is reduced: the cumulative probability at the centre of the circle is low in comparison to the other eigenstates. It would therefore seem that at low measurement strength there is less adherence to the Born rule.

Figures 11c and d are the same as a and b, respectively, but are displayed with a maximum cumulative probability density of 0.4 for the purpose of examining the paths followed by the system in greater detail. The avoided petal-like regions are clear in Figures 11b,c,d,e. For high measurement strength, illustrated in detail in Figure 11c, the cumulative probability density along the edges of the petals increases towards the $\langle S_x \rangle = \langle S_z \rangle = 0$ region and is higher than in the vicinities of the ± 1 eigenstates of the two observables. However, for a lower measurement strength, depicted in Figures 11b and d, the cumulative probability density spreads further away from the centre, creating a distinct region of exclusion around $\langle S_x \rangle = \langle S_z \rangle = 0$. For even lower measurement strength, shown in Figure 11e, the cumulative probability density is pushed further towards the circumference of the circle. This suggests that when measurement strength is low, the system tends to follow pathways that lead to collapse at the eigenstates of S_x and S_z that lie on the circumference of the circle rather than at the centre. At the lowest measurement strength, in Figure 11f, the petal patterns are hardly visible, suggesting that the two-step measurement cascade process is not so rigidly followed. In Figure 11f the system appears to collapse less often at

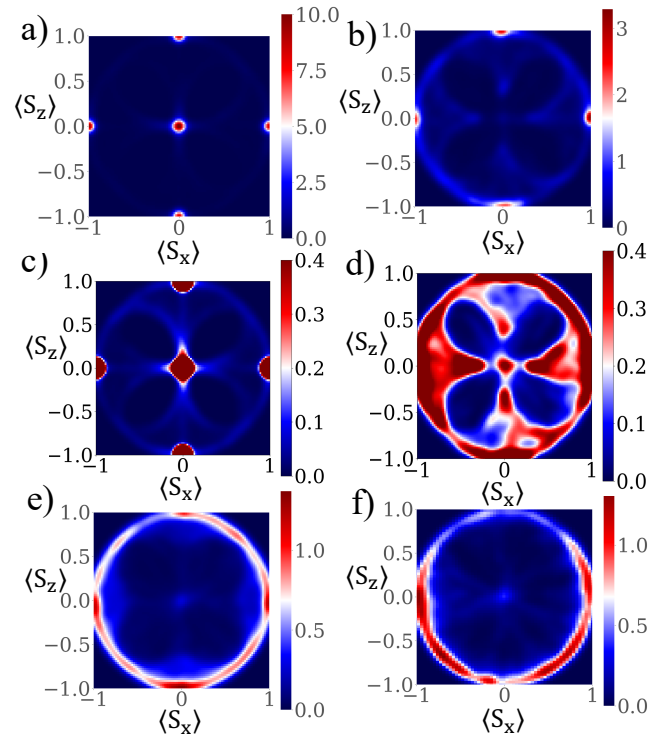


Figure 11. Color. Trajectories of the spin 1 system in terms of the spin components ($\langle S_x \rangle$, $\langle S_z \rangle$) are used to generate a cumulative probability density. Duration 500, time-step 0.0001. Measurement strengths for both observables: a) 8, b) 2, c) 8, d) 2, similarly with a range of probability density of 0-0.4 e) 1, f) 0.5.

the $| 1 \rangle_z$ and $| 0 \rangle_z$ eigenstates than at $| - 1 \rangle_z$, though this could be a result of insufficient sampling.

We can speculate about the reason for the lower frequency of visits to the $| 0 \rangle_x$ and $| 0 \rangle_z$ eigenstates during weak measurement compared with the strong measurement case. At low measurement strength, the system might not always be able to collapse at an eigenstate over the time-frame of the measurement. For weak measurement strength, Figure 12a illustrates collapse probabilities to the S_z eigenstates over the course of an S_z measurement and Figure 12b illustrates the collapse probabilities to the S_x eigenstates in a S_x measurement performed directly afterwards. The system reaches the vicinity of $| 0 \rangle_z$ after an S_z measurement. Since $| 0 \rangle_z$ written in the S_x basis ($| 0 \rangle_z = -\frac{1}{\sqrt{2}}| 1 \rangle_x + \frac{1}{\sqrt{2}}| - 1 \rangle_x$) suggests equal probabilities of collapse to $| 1 \rangle_x$ and $| - 1 \rangle_x$, the system then has a probability of collapse to $| 0 \rangle_x$ which is close to zero during the subsequent S_x measurement, depicted in Figure 12b. It therefore takes little time for the system to reach a state of superposition of just the $| 1 \rangle_x$ and $| - 1 \rangle_x$ eigenstates. In effect, the system is given a ‘head start’ in its collapse to the $| 1 \rangle_x$ and $| - 1 \rangle_x$ eigenstates since the probability of the $| 0 \rangle_x$ eigenstate at the

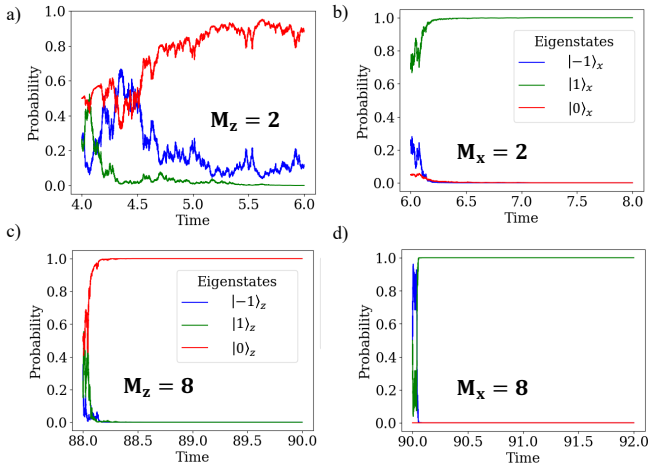


Figure 12. a) Collapse probabilities to the S_z eigenstates during an S_z measurement with measurement strength $M_z = 2$. b) Collapse probabilities of S_x eigenstates during an S_x measurement with measurement strength $M_x = 2$ that takes place directly after the evolution shown in a). c) As a) with measurement strength $M_z = 8$. d) As b) with measurement strength $M_x = 8$. Plots a) and c) share a legend, as do plots b) and d). Note that the selection of $|0\rangle_z$ in a) and c) takes longer than the selection of $|1\rangle_x$ in b) and d)

beginning of the S_z measurement was already very close to zero.

In contrast, if the system lies initially in the vicinity of a $|1\rangle_x$ or $| - 1\rangle_x$ eigenstate, the subsequent S_z measurement is a two-step process since probabilities of all three S_z eigenstates are substantial, for example $| - 1\rangle_x = \frac{1}{2}|1\rangle_z + \frac{1}{\sqrt{2}}|0\rangle_z + \frac{1}{2}| - 1\rangle_z$. The system has to dedicate a significant amount of time to the first stage of the measurement cascade, the arrival at a point on one of the two-eigenstate superposition loci. If the $|0\rangle_z$ eigenstate is accessible largely when the system starts an S_z measurement from $|\pm 1\rangle_x$ rather than $|0\rangle_x$ then its selection is always subject to this overhead, in contrast to the selection of $|\pm 1\rangle_x$ starting from $|0\rangle_z$. This might explain the less frequent visits to the zero eigenstates under weak measurement.

In the strong measurement case illustrated in Figures 12c,d, the system has ample time to complete a two-step collapse and therefore the eigenstates are explored in accordance with the Born rule statistics. The system takes around 0.22 time-units to reach either the $|1\rangle_z$ or the $| - 1\rangle_z$ eigenstates starting from $|0\rangle_x$ during an S_z measurement (based on 10,000 trajectories arriving at either of these eigenstates with $a_{max} = 1$). On the other hand, when starting in the superposition $\frac{1}{\sqrt{2}}(| - 1\rangle_z + |0\rangle_z)$ on the ellipse in the lower half of Figure 9a, the system takes 0.89 time-units to reach one of $| - 1\rangle_z$ or $|0\rangle_z$ during an S_z measurement. For a measurement interval of limited duration this suggests a greater likelihood for the system to arrive successfully at the $| - 1\rangle_z$ and $|1\rangle_z$ eigenstates compared with the $|0\rangle_z$ eigenstate.

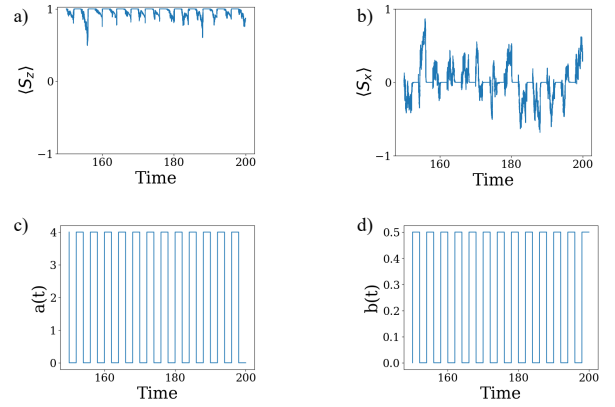


Figure 13. a) Evolution of $\langle S_z \rangle$: the system returns to the $|1\rangle_z$ eigenstate for more than 13 consecutive S_z measurements whilst undergoing a sequence of alternating measurements of S_z and S_x . b) Evolution of $\langle S_x \rangle$. c) The coupling coefficient $a(t)$ governing the S_z measurement. d) The coupling coefficient $b(t)$ governing the S_x measurement. S_z measurement strength $M_z = 32$; S_x measurement strength $M_x = 0.5$. Duration 200, time-step 0.0001.

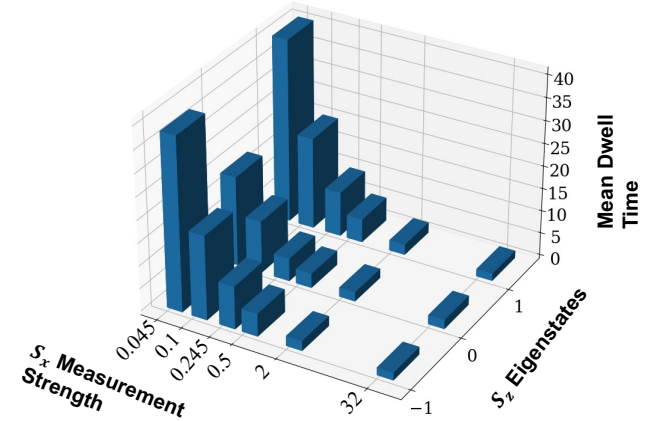


Figure 14. The mean dwell time for the three eigenstates of S_z at different S_x measurement strengths, for the spin 1 system. S_z measurement strength remains 32 throughout. The dwell time is the number of consecutive S_z measurements for which the system returns to the same eigenstate. Mean values based on a sequence of 5000 S_z measurements.

We now investigate dwell times for the spin 1 system. Figure 13 illustrates an example case where a sequence of strong S_z measurements and weak S_x measurements produces the return of the system to the $|1\rangle_z$ eigenstate on more than 13 consecutive occasions. This corresponds to a dwell time of over 13. Figure 14 depicts the mean dwell time for different S_x measurement strengths and for each eigenstate of S_z . The S_z measurement strength remains 32 for all cases.

Figure 14 shows how the mean dwell time at each of

the eigenstates of S_z increases as the S_x measurement strength is decreased. The mean dwell time appears to be the same for all three eigenstates of S_z at S_x measurement strengths 32 and 2, but for lower S_x measurement strengths the mean dwell time is higher for the $|\pm 1\rangle_z$ eigenstates than for the $|0\rangle_z$ eigenstate. This is a reflection of the decreased cumulative probability around the $|0\rangle_z$ eigenstate depicted in Figures 11b,d,e,f for low measurement strengths.

V. CONCLUSIONS

We have explored how memory of previous measurement outcomes may survive in a sequence of alternating measurements of non-commuting observables for a spin 1/2 system and a spin 1 system. We generate continuous, diffusive, stochastic quantum trajectories of the reduced density matrix ρ using the quantum state diffusion (QSD) formalism, treating measurement as a dynamical interaction between a system and an environment that is designed to act as a measurement apparatus. In order to model the sequence of measurements of observables S_x and S_z , we consider the system to interact with two environments with coupling coefficients $a(t)$ and $b(t)$ modelled as box functions in time, with $a(t) = 1, b(t) = 0$ and vice-versa. For the spin 1/2 system we generate trajectories in terms of the r_x, r_z components of the coherence vector representing the reduced density matrix. For the spin 1 system we illustrate trajectories in terms of the spin components $\langle S_x \rangle, \langle S_z \rangle$, where $\langle S_i \rangle = Tr(\rho S_i)$.

The spin 1/2 system is drawn towards the eigenstates of σ_x and σ_z that lie on the circumference of a Bloch sphere circle (Figure 4). The system typically travels between the eigenstates by remaining on the circle's circumference. The spin 1 system trajectories may also be represented on a circular space, though due to the greater number of eigenstates of the observables in question, the pattern is more complex, with the $|0\rangle_x$ and $|0\rangle_z$ eigenstates lying at the centre of the circle and the $|\pm 1\rangle_x$ and $|\pm 1\rangle_z$ eigenstates located on the circumference. We find that the system avoids certain regions of the (S_x, S_z) space, forming a petal-like pattern of cumulative probability.

This is an important feature of the measurement process of the spin 1 system, and we believe that it arises from a multistep process of collapse, a cascade of rejections of possible measurement outcomes until just one remains. The system typically starts a measurement process in a state with non-zero probability amplitudes for all three eigenstates of the observable in question. The probability amplitude of one of the eigenstates goes to zero, illustrated in Figure 10, drawing the system towards subspaces representing superpositions of pairs of eigenstates. The boundaries of the petal-like regions illustrated in Figure 9 correspond to these subspaces: the dynamics takes the system to these boundaries, but does not pass through them since to do so would be to undo

the partial collapse that has just been performed. Instead, the subsequent dynamics involves eliminating one or other of the remaining probability amplitudes, taking the system to an eigenstate, typically along edges of the petals.

We illustrate the behaviour for both systems using a cumulative probability density in Figures 6 and 11 which reveals that, as the measurement strength is decreased, the cumulative probability density deviates from that expected of the Born rule, which demands a strongly peaked probability density around the eigenstates of S_x and S_z . In particular, the probability density may be unevenly concentrated around certain eigenstates and not others, illustrating the system's tendency to return to the eigenstate it was in at the preceding measurement, demonstrated in Figures 5 and 13. For the spin 1 system the cumulative probability density around the $|0\rangle_x$ and $|0\rangle_z$ eigenstates decreases starkly as the measurement strength decreases, and is shifted towards the circumference of the circle where the other eigenstates of S_x and S_z reside.

Hence at low measurement strength there is a breakdown in the statistics predicted by the Born rule. The likely explanation is that an S_z measurement is relatively fast to complete when the system starts in $|0\rangle_x$, for which selection of $|\pm 1\rangle_z$ is favoured rather than $|0\rangle_z$. In contrast, completion of measurement is typically slower when the system starts in $|\pm 1\rangle_x$, which is the initial condition from which the $|0\rangle_z$ eigenstate is potentially reached. This effect arises from the near elimination of the first step in the multistep collapse process in the former situation.

Furthermore, memory of previous eigenstates of S_z in the sequence of alternating measurements of S_z and S_x can arise from an incomplete collapse to an eigenstate of S_x during a S_x measurement. Figures 5 and 13 demonstrate such a situation, where for several consecutive S_z measurements the system is able to return to the same eigenstate of S_z since the system has failed to collapse to an S_x eigenstate. To explore this further we consider sequences of alternating measurements with strong S_z measurements and weak S_x measurements. We calculate the mean dwell time for each eigenstate of S_z for varying S_x measurement strength. We define the dwell time as the number of consecutive S_z measurements for which the system is able to return to the same eigenstate of S_z .

Figure 14 shows how the mean dwell times for the spin 1/2 system increase with decreasing σ_x measurement strength, with high σ_z measurement strength throughout. The mean dwell times appear to be roughly equal for both eigenstates of σ_z . This is in accordance with the idea that at low measurement strength the system does not have enough time to collapse at a σ_x eigenstate and therefore memory of previous σ_z outcomes is not completely erased. The system remembers, and can return to, the same σ_z eigenstate it was in previously.

For the spin 1 system, the mean dwell time depicted in Figure 14 is more complicated. The mean dwell time

increases with decreasing S_x measurement strength. But whereas at high S_x measurement strengths the mean dwell time is equal for all three eigenstates of S_z , at lower S_x measurement strengths it is higher for the $|\pm 1\rangle_z$ eigenstates than for the $|0\rangle_z$ eigenstate. This is reflected in Figures 5 b-d. We suggest this could be due to the delicate measurement dynamics of the $|0\rangle_z$ eigenstate which lead to it being visited less frequently than the other two eigenstates.

Sequences of measurements of non-commuting observables have been performed experimentally with weak measurements [10, 15, 59], and we envisage that the investigations outlined in this work could also be tested experimentally. In addition, wavefunction collapse has been experimentally observed in real-time, offering insight into the measurement timescale required to successfully complete a measurement [30, 31].

In summary, memory of previous outcomes in a sequence of alternating measurements of non-commuting observables undergoing weak measurements could arise if there is insufficient time for the system to collapse to an eigenstate of the second non-commuting observable, introducing bias towards a return to the eigenstate of the

first non-commuting observable visited previously. This could operate in a similar spirit to the incomplete measurements exhibited in the partial quantum Zeno effect [65, 66] or reversed measurements, where the initial quantum state of the system is recovered after a partial measurement collapse [31, 67–69]. As such, our findings could be useful in fields of quantum state control such as quantum computation and cybersecurity protocols, quantum state tomography, as well as quantum error correction protocols where sequences of non-commuting observables are utilised. The avoidance of the $|0\rangle_x$ and $|0\rangle_z$ eigenstates of the S_x and S_z observables for the spin 1 system could also be of interest in quantum state control.

ACKNOWLEDGEMENTS

SMW is supported by a PhD studentship funded by EPSRC under grant codes EP/R513143/1 and EP/T517793/1. We thank the referee for their very insightful and useful comments.

-
- [1] T. Norsen, *Foundations of Quantum Mechanics: An Exploration of the Physical Meaning of Quantum Theory* (Springer, Cham, Switzerland, 2017).
 - [2] M. A. Nielsen and I. Chuang, Quantum Computation and Quantum Information, *American Journal of Physics* **70**, 558 (2002).
 - [3] Y. Pan, E. Cohen, E. Karimi, A. Gover, N. Schönberger, T. Chlouba, K. Wang, S. Nehemia, P. Hommelhoff, I. Kaminer, and Y. Aharonov, Weak measurements and quantum-to-classical transitions in free electron-photon interactions, *Light: Science & Applications* **12**, 267 (2023).
 - [4] L. A. Rozema, A. Darabi, D. H. Mahler, A. Hayat, Y. Soudagar, and A. M. Steinberg, Violation of Heisenberg’s Measurement-Disturbance Relationship by Weak Measurements, *Physical Review Letters* **109**, 100404 (2012).
 - [5] M. Malik, M. Mirhosseini, M. P. J. Lavery, J. Leach, M. J. Padgett, and R. W. Boyd, Direct measurement of a 27-dimensional orbital-angular-momentum state vector, *Nature Communications* **5**, 3115 (2014).
 - [6] J. S. Lundeen, B. Sutherland, A. Patel, C. Stewart, and C. Bamber, Direct Measurement of the Quantum Wavefunction, *Nature* **474**, 188 (2011).
 - [7] J. S. Lundeen and A. M. Steinberg, Experimental Joint Weak Measurement on a Photon Pair as a Probe of Hardy’s Paradox, *Physical Review Letters* **102**, 020404 (2009).
 - [8] J. S. Lundeen and C. Bamber, Procedure for Direct Measurement of General Quantum States Using Weak Measurement, *Physical Review Letters* **108**, 070402 (2012).
 - [9] O. Hosten and P. Kwiat, Observation of the Spin Hall Effect of Light via Weak Measurements, *Science* **319**, 787 (2008).
 - [10] F. Piacentini, A. Avella, M. P. Levi, R. Lussana, F. Villa, A. Tosi, F. Zappa, M. Gramegna, G. Brida, I. P. Degiovanni, and M. Genovese, Experiment Investigating the Connection between Weak Values and Contextuality, *Physical Review Letters* **116**, 180401 (2016).
 - [11] O. Calderón-Losada, T. T. Moctezuma Quistian, H. Cruz-Ramirez, S. Murgueitio Ramirez, A. B. U’Ren, A. Botero, and A. Valencia, A Weak Values Approach for Testing Simultaneous Einstein–Podolsky–Rosen Elements of Reality for Non-Commuting Observables, *Communications Physics* **3**, 1 (2020).
 - [12] A. Chantasri, J. Atalaya, S. Hacoheh-Gourgy, L. S. Martin, I. Siddiqi, and A. N. Jordan, Simultaneous Continuous Measurement of Noncommuting Observables: Quantum State Correlations, *Physical Review A* **97**, 012118 (2018).
 - [13] J. Atalaya, S. Hacoheh-Gourgy, L. S. Martin, I. Siddiqi, and A. N. Korotkov, Correlators in Simultaneous Measurement of Non-Commuting Qubit Observables, *npj Quantum Information* **4**, 1 (2018).
 - [14] A. N. Jordan and M. Büttiker, Continuous Quantum Measurement with Independent Detector Cross Correlations, *Physical Review Letters* **95**, 220401 (2005).
 - [15] Y. Suzuki, M. Inuma, and H. F. Hofmann, Observation of Non-Classical Correlations in Sequential Measurements of Photon Polarization, *New Journal of Physics* **18**, 103045 (2016).
 - [16] F. Piacentini, A. Avella, M. P. Levi, M. Gramegna, G. Brida, I. P. Degiovanni, E. Cohen, R. Lussana, F. Villa, A. Tosi, F. Zappa, and M. Genovese, Measuring Incompatible Observables by Exploiting Sequential Weak Values, *Physical Review Letters* **117**, 170402 (2016).
 - [17] Y. Suzuki, M. Inuma, and H. F. Hofmann, Violation of Leggett–Garg Inequalities in Quantum Measurements

- with Variable Resolution and Back-Action, *New Journal of Physics* **14**, 103022 (2012).
- [18] J. Dressel, C. J. Broadbent, J. C. Howell, and A. N. Jordan, Experimental Violation of Two-Party Leggett-Garg Inequalities with Semiweak Measurements, *Physical Review Letters* **106**, 040402 (2011).
- [19] M. E. Goggin, M. P. Almeida, M. Barbieri, B. P. Lanyon, J. L. O'Brien, A. G. White, and G. J. Pryde, Violation of the Leggett-Garg inequality with weak measurements of photons, *Proceedings of the National Academy of Sciences* **108**, 1256 (2011).
- [20] N. S. Williams and A. N. Jordan, Weak Values and the Leggett-Garg Inequality in Solid-State Qubits, *Physical Review Letters* **100**, 026804 (2008).
- [21] A. Palacios-Laloy, F. Mallet, F. Nguyen, P. Bertet, D. Vion, D. Esteve, and A. N. Korotkov, Experimental Violation of a Bell's Inequality in Time with Weak Measurement, *Nature Physics* **6**, 442 (2010).
- [22] A. Kulikov, M. Jerger, A. Potočník, A. Wallraff, and A. Fedorov, Realization of a Quantum Random Generator Certified with the Kochen-Specker Theorem, *Physical Review Letters* **119**, 240501 (2017).
- [23] C. Simon, M. Żukowski, H. Weinfurter, and A. Zeilinger, Feasible "Kochen-Specker" Experiment with Single Particles, *Physical Review Letters* **85**, 1783 (2000).
- [24] Y.-F. Huang, C.-F. Li, Y.-S. Zhang, J.-W. Pan, and G.-C. Guo, Experimental Test of the Kochen-Specker Theorem with Single Photons, *Physical Review Letters* **90**, 250401 (2003).
- [25] J. C. Howell, R. S. Bennink, S. J. Bentley, and R. W. Boyd, Realization of the Einstein-Podolsky-Rosen Paradox Using Momentum- and Position-Entangled Photons from Spontaneous Parametric Down Conversion, *Physical Review Letters* **92**, 210403 (2004).
- [26] L. P. García-Pintos and J. Dressel, Probing Quantumness with Joint Continuous Measurements of Noncommuting Qubit Observables, *Physical Review A* **94**, 062119 (2016).
- [27] M. Sindelka and N. Moiseyev, Quantum Uncertainties and Heisenberg-like Uncertainty Relations for a Weak Measurement Scheme Involving Two Arbitrary Noncommuting Observables, *Physical Review A* **97**, 012122 (2018).
- [28] S. Hossenfelder, Testing Super-Deterministic Hidden Variables Theories, *Foundations of Physics* **41**, 1521 (2011).
- [29] Z. K. Mineev, S. O. Mundhada, S. Shankar, P. Reinhold, R. Gutiérrez-Jáuregui, R. J. Schoelkopf, M. Mirrahimi, H. J. Carmichael, and M. H. Devoret, To Catch and Reverse a Quantum Jump Mid-Flight, *Nature* **570**, 200 (2019).
- [30] A. N. Jordan, Watching the Wavefunction Collapse, *Nature* **502**, 177 (2013).
- [31] K. W. Murch, S. J. Weber, C. Macklin, and I. Siddiqi, Observing Single Quantum Trajectories of a Superconducting Quantum Bit, *Nature* **502**, 211 (2013).
- [32] J. Gambetta, A. Blais, M. Boissonneault, A. A. Houck, D. I. Schuster, and S. M. Girvin, Quantum trajectory approach to circuit QED: Quantum jumps and the Zeno effect, *Physical Review A* **77**, 012112 (2008).
- [33] C. Gneiting, A. V. Rozhkov, and F. Nori, Jump-Time Unraveling of Markovian Open Quantum Systems, *Physical Review A* **104**, 062212 (2021).
- [34] M. B. Plenio and P. L. Knight, The Quantum-Jump Approach to Dissipative Dynamics in Quantum Optics, *Reviews of Modern Physics* **70**, 101 (1998).
- [35] Y. Tanimura, Real-Time and Imaginary-Time Quantum Hierarchical Fokker-Planck Equations, *The Journal of Chemical Physics* **142**, 144110 (2015).
- [36] G. Lindblad, On the Generators of Quantum Dynamical Semigroups, *Communications in Mathematical Physics* **48**, 119 (1976).
- [37] I. de Vega and D. Alonso, Dynamics of non-Markovian open quantum systems, *Reviews of Modern Physics* **89**, 015001 (2017).
- [38] R. P. Feynman and F. L. Vernon, The theory of a general quantum system interacting with a linear dissipative system, *Annals of Physics* **24**, 118 (1963).
- [39] T. Li, Y. Yan, and Q. Shi, A low-temperature quantum Fokker-Planck equation that improves the numerical stability of the hierarchical equations of motion for the Brownian oscillator spectral density, *The Journal of Chemical Physics* **156**, 064107 (2022).
- [40] H. M. Wiseman and G. J. Milburn, Interpretation of quantum jump and diffusion processes illustrated on the Bloch sphere, *Physical Review A* **47**, 1652 (1993).
- [41] W. S. Teixeira, F. L. Semião, J. Tuorila, and M. Möttönen, Assessment of Weak-Coupling Approximations on a Driven Two-Level System under Dissipation, *New Journal of Physics* **24**, 013005 (2021).
- [42] A. Chantasri and A. N. Jordan, Stochastic Path-Integral Formalism for Continuous Quantum Measurement, *Physical Review A* **92**, 032125 (2015).
- [43] I. Percival, *Quantum State Diffusion* (Cambridge University Press, Cambridge, 1998).
- [44] N. Gisin and I. C. Percival, The quantum-state diffusion model applied to open systems, *Journal of Physics A: Mathematical and General* **25**, 5677 (1992).
- [45] H. M. Wiseman, Quantum Trajectories and Quantum Measurement Theory, *Quantum and Semiclassical Optics: Journal of the European Optical Society Part B* **8**, 205 (1996).
- [46] K. Jacobs, *Quantum Measurement Theory and Its Applications* (Cambridge University Press, Cambridge, 2014).
- [47] S. M. Walls, J. M. Schachter, H. Qian, and I. J. Ford, Stochastic quantum trajectories demonstrate the quantum Zeno effect in open spin 1/2, spin 1 and spin 3/2 systems, *Journal of Physics A: Mathematical and Theoretical* **57**, 175301 (2024).
- [48] N. Gisin and I. C. Percival, *Quantum State Diffusion: From Foundations to Applications* (1997).
- [49] G. S. Thekkadath, L. Giner, Y. Chalich, M. J. Horton, J. Banker, and J. S. Lundeen, Direct Measurement of the Density Matrix of a Quantum System, *Physical Review Letters* **117**, 120401 (2016).
- [50] R. Ber, S. Marcovitch, O. Kenneth, and B. Reznik, Process Tomography for Systems in a Thermal State, *New Journal of Physics* **15**, 013050 (2013).
- [51] A. Brodutch and E. Cohen, A Scheme for Performing Strong and Weak Sequential Measurements of Non-Commuting Observables, *Quantum Studies: Mathematics and Foundations* **4**, 13 (2017).
- [52] Y. Kim, Y.-S. Kim, S.-Y. Lee, S.-W. Han, S. Moon, Y.-H. Kim, and Y.-W. Cho, Direct Quantum Process Tomography via Measuring Sequential Weak Values of Incompatible Observables, *Nature Communications* **9**, 192 (2018).

- [53] C. L. Clarke and I. J. Ford, Stochastic Entropy Production Associated with Quantum Measurement in a Framework of Markovian Quantum State Diffusion (2023).
- [54] J. Atalaya, M. Bahrami, L. P. Pryadko, and A. N. Korotkov, Bacon-Shor Code with Continuous Measurement of Noncommuting Operators, *Physical Review A* **95**, 032317 (2017).
- [55] M. Berta, M. Christandl, R. Colbeck, J. M. Renes, and R. Renner, The Uncertainty Principle in the Presence of Quantum Memory, *Nature Physics* **6**, 659 (2010).
- [56] M. N. Bera, A. Acín, M. Kuś, M. W. Mitchell, and M. Lewenstein, Randomness in Quantum Mechanics: Philosophy, Physics and Technology, *Reports on Progress in Physics* **80**, 124001 (2017).
- [57] R. Prevedel, D. R. Hamel, R. Colbeck, K. Fisher, and K. J. Resch, Experimental Investigation of the Uncertainty Principle in the Presence of Quantum Memory and Its Application to Witnessing Entanglement, *Nature Physics* **7**, 757 (2011).
- [58] S. Hacoheh-Gourgy, L. S. Martin, E. Flurin, V. V. Ramasesh, K. B. Whaley, and I. Siddiqi, Quantum Dynamics of Simultaneously Measured Non-Commuting Observables, *Nature* **538**, 491 (2016).
- [59] H. F. Hofmann, Sequential Measurements of Non-Commuting Observables with Quantum Controlled Interactions, *New Journal of Physics* **16**, 063056 (2014).
- [60] J.-S. Chen, M.-J. Hu, X.-M. Hu, B.-H. Liu, Y.-F. Huang, C.-F. Li, C.-G. Guo, and Y.-S. Zhang, Experimental Realization of Sequential Weak Measurements of Non-Commuting Pauli Observables, *Optics Express* **27**, 6089 (2019).
- [61] G. Mitchison, R. Jozsa, and S. Popescu, Sequential Weak Measurement, *Physical Review A* **76**, 062105 (2007).
- [62] M. A. Ochoa, W. Belzig, and A. Nitzan, Simultaneous Weak Measurement of Non-Commuting Observables: A Generalized Arthurs-Kelly Protocol, *Scientific Reports* **8**, 15781 (2018).
- [63] M. Ozawa, Universally Valid Reformulation of the Heisenberg Uncertainty Principle on Noise and Disturbance in Measurement, *Physical Review A* **67**, 042105 (2003).
- [64] R. Ruskov, A. N. Korotkov, and K. Mølmer, Qubit State Monitoring by Measurement of Three Complementary Observables, *Physical Review Letters* **105**, 100506 (2010).
- [65] A. Peres and A. Ron, Incomplete “collapse” and Partial Quantum Zeno Effect, *Physical Review A* **42**, 5720 (1990).
- [66] M. Zhang, C. Wu, Y. Xie, W. Wu, and P. Chen, Quantum Zeno Effect by Incomplete Measurements, *Quantum Information Processing* **18**, 97 (2019).
- [67] N. Katz, M. Neeley, M. Ansmann, R. C. Bialczak, M. Hofheinz, E. Lucero, A. O’Connell, H. Wang, A. N. Cleland, J. M. Martinis, and A. N. Korotkov, Reversal of the Weak Measurement of a Quantum State in a Superconducting Phase Qubit, *Physical Review Letters* **101**, 200401 (2008).
- [68] A. N. Korotkov and A. N. Jordan, Undoing a Weak Quantum Measurement of a Solid-State Qubit, *Physical Review Letters* **97**, 166805 (2006).
- [69] Y.-S. Kim, J.-C. Lee, O. Kwon, and Y.-H. Kim, Protecting Entanglement from Decoherence Using Weak Measurement and Quantum Measurement Reversal, *Nature Physics* **8**, 117 (2012).
- [70] D. M. Tong, J.-L. Chen, L. C. Kwek, and C. H. Oh, Kraus Representation for Density Operator of Arbitrary Open Qubit System, *Laser Physics* **16**, 1512 (2006).
- [71] D. Matos, L. Kantorovich, and I. J. Ford, Stochastic Entropy Production for Continuous Measurements of an Open Quantum System (2022).
- [72] J. A. Gross, C. M. Caves, G. J. Milburn, and J. Combes, Qubit Models of Weak Continuous Measurements: Markovian Conditional and Open-System Dynamics, *Quantum Science and Technology* **3**, 024005 (2018).
- [73] C. L. Clarke, *Irreversibility Measures in a Quantum Setting*, Doctoral, UCL (University College London) (2022).

Appendix A: Spin 1 density matrix and SDEs

The Gell-Mann matrices used to form the spin 1 density matrix are as follows:

$$\begin{aligned} \lambda_1 &= \begin{pmatrix} 0 & 1 & 0 \\ 1 & 0 & 0 \\ 0 & 0 & 0 \end{pmatrix} & \lambda_2 &= \begin{pmatrix} 0 & -i & 0 \\ i & 0 & 0 \\ 0 & 0 & 0 \end{pmatrix} & \lambda_3 &= \begin{pmatrix} 1 & 0 & 0 \\ 0 & -1 & 0 \\ 0 & 0 & 0 \end{pmatrix} \\ \lambda_4 &= \begin{pmatrix} 0 & 0 & 1 \\ 0 & 0 & 0 \\ 1 & 0 & 0 \end{pmatrix} & \lambda_5 &= \begin{pmatrix} 0 & 0 & -i \\ 0 & 0 & 0 \\ i & 0 & 0 \end{pmatrix} & \lambda_6 &= \begin{pmatrix} 0 & 0 & 0 \\ 0 & 0 & 1 \\ 0 & 1 & 0 \end{pmatrix} \\ \lambda_7 &= \begin{pmatrix} 0 & 0 & 0 \\ 0 & 0 & -i \\ 0 & i & 0 \end{pmatrix} & \lambda_8 &= \frac{1}{\sqrt{3}} \begin{pmatrix} 1 & 0 & 0 \\ 0 & 1 & 0 \\ 0 & 0 & -2 \end{pmatrix}. \end{aligned} \quad (\text{A1})$$

A parametrisation of the density matrix for the spin 1 system then emerges:

$$\rho = \frac{1}{3} \begin{pmatrix} 1 + \sqrt{3}u + z & -i\sqrt{3}m + \sqrt{3}s & \sqrt{3}v - i\sqrt{3}k \\ i\sqrt{3}m + \sqrt{3}s & 1 - \sqrt{3}u + z & \sqrt{3}x - i\sqrt{3}y \\ \sqrt{3}v + i\sqrt{3}k & \sqrt{3}x + i\sqrt{3}y & 1 - 2z \end{pmatrix}. \quad (\text{A2})$$

Stochastic quantum trajectories can be produced from the equations of motion for the eight variables parametrising ρ . These are generated from

$$dR_i = \frac{\sqrt{3}}{2} \text{Tr}(d\rho\lambda_i), \quad (\text{A3})$$

using the properties of the Gell-Mann matrices. The components of the coherence vector \mathbf{R} defined in section IIIB are denoted R_i .

The SDEs for the variables parametrising the spin 1 density matrix are as follows:

$$\begin{aligned}
dk &= -2a^2kdt - \frac{1}{2}b^2kdt + a\left(-\frac{2}{\sqrt{3}}ku - 2kz\right)dW_z + b\left(-\frac{2\sqrt{2}}{\sqrt{3}}ks - \frac{2\sqrt{2}}{\sqrt{3}}kx + \frac{1}{\sqrt{2}}m + \frac{1}{\sqrt{2}}y\right)dW_x \\
dm &= -\frac{1}{2}a^2mdt + b^2\left(\frac{3}{4}y - \frac{5}{4}m\right)dt - a\left(\frac{2}{\sqrt{3}}mu - 2mz + zm\right)dW_z + b\left(\frac{1}{\sqrt{2}}k - \frac{2\sqrt{2}}{\sqrt{3}}ms - \frac{2\sqrt{2}}{\sqrt{3}}mx\right)dW_x \\
ds &= -\frac{1}{2}a^2sdt + \frac{1}{4}b^2(x-s)dt + a\left(-\frac{2}{\sqrt{3}}su - 2sz + s\right)dW_z + b\left(-\frac{2\sqrt{2}}{\sqrt{3}}s^2 - \frac{2\sqrt{2}}{\sqrt{3}}sx + \frac{1}{\sqrt{2}}v + \frac{\sqrt{2}}{\sqrt{3}}z + \frac{\sqrt{2}}{\sqrt{3}}\right)dW_x \\
du &= b^2\left(-\frac{5}{4}u - \frac{3}{4}v + \frac{\sqrt{3}}{4}z\right)dt + a\left(-\frac{2}{\sqrt{3}}u^2 - 2uz + zu + \frac{1}{\sqrt{3}}z + \frac{1}{\sqrt{3}}\right)dW_z + b\left(-\frac{2\sqrt{2}}{\sqrt{3}}su - \frac{2\sqrt{2}}{\sqrt{3}}ux - \frac{1}{\sqrt{2}}x\right)dW_x \\
dv &= -2a^2vdt + b^2\left(-\frac{1}{2}v - \frac{3}{4}u + \frac{\sqrt{3}}{4}z\right)dt + a\left(-\frac{2}{\sqrt{3}}uv - 2vz\right)dW_z + b\left(\frac{2\sqrt{2}}{\sqrt{3}}sv + \frac{1}{\sqrt{2}}s - \frac{2\sqrt{2}}{\sqrt{3}}vx + \frac{1}{\sqrt{2}}x\right)dW_x \\
dx &= -\frac{1}{2}a^2xdt + b^2\left(\frac{1}{4}s - \frac{1}{4}x\right)dt - a\left(\frac{2}{\sqrt{3}}ux + 2xz + x\right)dW_z + \frac{\sqrt{2}}{\sqrt{3}}b\left(-2sx - \frac{\sqrt{3}}{2}u + \frac{\sqrt{3}}{2}v - 2x^2 - \frac{1}{2}z + 1\right)dW_x \\
dy &= -\frac{1}{2}a^2ydt + b^2\left(\frac{3}{4}m - \frac{5}{4}y\right)dt + a\left(-\frac{2}{\sqrt{3}}uy - 2yz - y\right)dW_z + b\left(\frac{1}{\sqrt{2}}k - \frac{2\sqrt{2}}{\sqrt{3}}sy - \frac{2\sqrt{2}}{\sqrt{3}}xy\right)dW_x \\
dz &= b^2\left(\frac{\sqrt{3}}{4}u + \frac{\sqrt{3}}{4}v - \frac{3}{4}z\right)dt + a\left(-\frac{2}{\sqrt{3}}uz + \frac{1}{\sqrt{3}}u - 2z^2 - z + 1\right)dW_z + \frac{\sqrt{2}}{\sqrt{3}}b\left(-2sz + s - 2xz - \frac{1}{2}x\right)dW_x
\end{aligned} \tag{A4}$$
